Optics Communications 282 (2009) 1148–1153

Contents lists available at ScienceDirect

Optics Communications

journal homepage: www.elsevier.com/locate/optcom

Photoluminescence of colloidal YVO_4:Eu/SiO_2 core/shell nanocrystals

Yan Wang [b], Weiping Qin [a,b,*], Jisen Zhang [b], Chunyan Cao [b], Shaozhe Lü [b], Xinguang Ren [b]

[a] State Key Laboratory on Integrated Optoelectronics, College of Electronic Science and Engineering, Jilin University, 2699 Qianjin Street, Changchun 130012, China
[b] Key Laboratory of Excited State Processes, Changchun Institute of Optics, Fine Mechanics and Physics, Chinese Academy of Sciences, Changchun 130033, China

ARTICLE INFO

Article history:
Received 30 May 2008
Received in revised form 8 September 2008
Accepted 3 December 2008

Keywords:
Photoluminescence
YVO_4:Eu/SiO_2
Core/shell
Nanocrystals
Laser selective excitation

ABSTRACT

YVO_4:Eu, and YVO_4:Eu/SiO_2 nanocrystals (NCs) were prepared by hydrothermal method with citrate as capping ligands. Their morphologies, structures, components, and photoluminescence properties were investigated and presented in this paper. A remarkable fluorescence enhancement up to 2.17 times was observed in colloidal YVO_4:Eu/SiO_2 NCs, compared to that of colloidal YVO_4:Eu NCs. This is mainly attributed to the formation of the outer protecting layers of biocompatible SiO_2 shells; which shield the Eu^{3+} ions effectively from water and thus reduces the deleterious effects of water on the luminescence. Meanwhile, on the basis of laser selective excitation, two kinds of luminescent centers were confirmed in the NCs, namely, inner Eu^{3+} ions and surface Eu^{3+} ions. The surface modifications for YVO_4:Eu NCs effectively reduced the surface defects and accordingly enhanced the luminescence. The core/shell NCs exhibited long fluorescence lifetime and high photostability under ultraviolet radiation.

1. Introduction

The Eu^{3+}-activated Yttrium orthovanadate (YVO_4), a well-known rare-earth (RE) doped inorganic luminescent materials, has been used as an important commercial red phosphor owing to its high luminescence efficiency on electron-beam excitation since 1964 [1]. Recently, considerable efforts have been devoted to develop the different synthesis methods for preparation of luminescent colloidal YVO_4:Eu NCs. Huignard et al. achieved transparent aqueous dispersions of 10 nm sized YVO_4:Eu NCs based on the aqueous precipitation reaction by the addition of a citrate ligand [2]. Haase et al. obtained different rare-earth ions doped colloidal YVO_4 NCs with the size range from 10 to 30 nm via hydrothermal method [3–4]. Other methods such as microwave irradiation [5], microemulsion [6] have also been adopted in the preparation of colloidal YVO_4:Eu NCs. For RE doped nanophosphors, a very important application is to exploit them as fluorescence probes in biological fields such as immunoassaying, DNA sequencing, and clinical diagnosing. Water-solubility is necessary to exploit the applications of RE doped nanophosphors in biology.

However, one problem, arising from the absorption of surface OH^- and water molecules, is frequently encountered when NCs are dispersed into aqueous environment. The OH^- group has a high vibration frequency and can efficiently quench the luminescence of RE ions [7–11]. Meanwhile, various defects on the surface of NCs, such as dangling bonds and disorder, also greatly decrease the luminescent intensity of nanophorphors [12–16]. Fortunately, these problems can be overcome when an appropriate shell is grown around the core. Silica is usually used as a coating material due to its high chemical stability, optical transparency, easy controllable shell thickness, and biocompatibility [17]. For example, Nann et al. has successfully synthesized YVO_4:Eu/SiO_2 core/shell nanocrystals in microemulsion [18]. In this paper, we synthesized water-soluble YVO_4:Eu colloidal NCs via hydrothermal method followed by coating with silica shell, and then we noticed their luminescence enhancement of 2.17 times. We then used the laser selective excitation spectra to study the surface modification effect on the photoluminescence of YVO_4:Eu and YVO_4:Eu/SiO_2 NCs.

2. Experimental

All the chemicals utilized in the synthesis were of analytical grade and were used as received without any purification. Rare-earth chemicals were obtained from Shanghai Yuelong New Materials Co., Ltd. The other chemicals were purchased from Beijing Chemical Reagent Company.

The YVO_4:Eu NCs were synthesized with similar hydrothermal methods reported in literature [2,3]. In a water bath at 60 °C, a 2 ml aqueous solution containing $Y(NO_3)_3{\cdot}6H_2O$ (0.95 mmol) and $Eu(NO_3)_3 \cdot 6H_2O$ (0.05 mmol) was mixed with another aqueous solution (2 ml) containing 0.22 g citrate sodium under vigorous stirring, and a white precipitate of lanthanide citrate was formed. An aqueous solution of Na_3VO_4 (0.1 mmol, pH 12.7) was then

* Corresponding author. Address: State Key Laboratory on Integrated Optoelectronics, College of Electronic Science and Engineering, Jilin University, 2699 Qianjin Street, Changchun 130012, China. Tel./fax: +86 431 85168240-8325.
E-mail address: wpqin@jlu.edu.cn (W. Qin).

0030-4018/$ - see front matter © 2008 Elsevier B.V. All rights reserved.
doi:10.1016/j.optcom.2008.12.007

added dropwise to the mixture until the precipitate was completely dissolved. After being stirred for 1 h, the resulting clear precursor solution was transferred to a 50 ml autoclave for hydrothermal treatment at 200 °C for 10 h followed by cooling in the furnace. The precipitate of YVO_4:Eu NCs was separated by centrifugation and then washed with deionized water and ethanol several times.

Stöber method was adopted for the SiO_2 coating process [19]. 50 mg YVO_4:Eu NCs were dispersed in a mixture of distilled water (1.5 ml) and ethanol (20 ml). Then 400 μl of NH_4OH (25%) were added in the solution under stirring. After mixing for 10 min, 200-μl tetraethyl orthosilicate (TEOS) was added dropwise to the mixture. The mixture was stirred for 3 h. White-colored silica-coated YVO_4:Eu NCs were centrifuged and washed with ethanol for several times and then dried in vacuum.

The size and morphology of NCs were characterized by TEM (JEM, 2000EX 200KV). The sample for TEM observation was prepared by placing a drop of diluted water dispersion of NCs onto copper grid supported by a holey carbon film. Phase identification was performed via powder X-ray diffraction (XRD) (Rigaku RU-200b) with Cu Kα radiation ($\lambda = 1.5406$ Å). The XPS spectra for powder samples were recorded on an ESCALAB MK II X-ray photoelectron spectrometer from VG Co. with Al Kα radiation. Infrared spectra with range of 400–4000 cm^{-1} were obtained on a Bio-Rad Fourier transform infrared spectrometer with fresh KBr pellets. The UV–vis absorption spectra were recorded by a UV–vis-NIR scanning spectrophotometer (SHIMADZU). Room-temperature excitation and emission spectra were performed with a Hitachi F-4500 fluorescence spectrometer equipped with a continuous 150 W Xe-arc lamp. For comparing the intensities of different samples, the emission spectra were measured with the same instrument parameters (2.5 nm for excitation slit, 2.5 nm for emission slit, and 700 V for PMT voltage). High-resolution emission spectra and laser selective excitation spectra (luminescence decay curves were measure at room-temperature) were performed at 10 K with the samples mounted in a helium exchange gas chamber of a closed cycle refrigeration system. A pulsed Nd:YAG laser equipped with second (532 nm), third (355 nm), and fourth (266 nm) harmonic generators was used as excitation source, which has a line width of 0.2 cm^{-1}, pulse duration of 10 ns, and repetition frequency of 10 Hz. A Rodamine 6 G dye laser pumped by the 532-nm beam was used for site-selective excitation. High-resolution spectra were recorded on a Spex 1403 spectrometer, and photoluminescence signals were detected by a photomultiplier (R955), averaged with a gated boxcar integrator, and processed by a personal computer. The fluorescence photo of colloidal NCs with 0.125 mg/ml concentration in water was acquired with a digital camera under 254-nm excitation from an UV lamp.

3. Results and discussion

Fig. 1 shows the powder X-ray diffraction (XRD) patterns of YVO_4:Eu, and YVO_4:Eu/SiO_2 NCs. Both of these patterns could be readily indexed with tetragonal cells of $a \sim 7.12$ Å and $c \sim 6.29$ Å, which match well the record of JCPDS 17-0341. The indexes are included in the figure. It proved that we have successfully synthesized the pure YVO_4 phase.

From the Fig. 2A, one can see that most YVO_4:Eu NCs present tetragonal-like morphology with average size of 30-nm. Fig. 2B shows that the silica-coated YVO_4:Eu NCs have clear core/shell structures. The selected area electron diffraction (SAED) patterns of the YVO_4:Eu and YVO_4:Eu/SiO_2 NCs (insets in Fig. 2A, and B, respectively) show some discrete spots and even rings. The d spaces calculated for both patterns match well with our XRD results, which confirmed that our particles are nano scaled YVO_4 phase. We then use XPS (X-ray photoelectron spectra) to determine the surface composition of our samples. As shown in Fig. 3, the peaks of binding energy from the Eu (3d) can be clearly seen in YVO_4:Eu NCs and the europium concentration is 4.9%. However, the peak of Eu (3d) cannot be detected in YVO_4:Eu/SiO_2 NCs due to the cover of the SiO_2 shell, whereas the peak of Si (2p) is obvious, indicating that Si compound is coated on the particles (Fig. 3). This result is in good agreement with TEM observation of YVO_4:Eu/SiO_2 NCs. It is worth mentioning that the binding energy of O (1s) shifts to high-energy side in YVO_4:Eu /SiO_2 NCs (Fig. 3). Compared with O (1s) peaks of YVO_4:Eu NCs, there is a chemical shift of 2.7 eV. The difference in binding energy came from the structure difference, i.e., O (1s) peaks of YVO_4:Eu NCs is assigned to the lattice oxygen, while the O (1s) peak of YVO_4:Eu/SiO_2 is assigned to the oxygen of Si–OH [20–22].

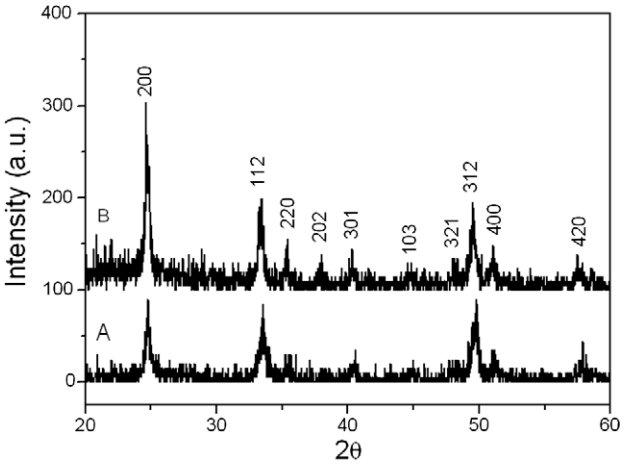

Fig. 1. XRD patterns of YVO_4:Eu (A) and YVO_4:Eu/SiO_2 (B) NCs.

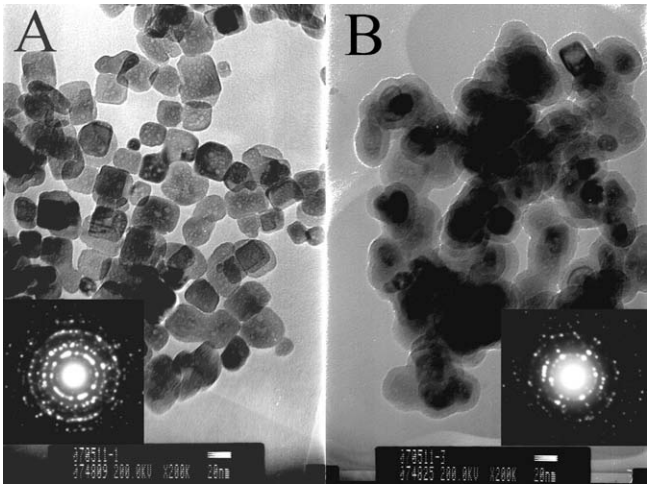

Fig. 2. TEM images of YVO_4:Eu (A) and YVO_4:Eu/SiO_2 (B) NCs. The scale bar is 20 nm and the insets display the SAED patterns.

Fig. 4 shows the Fourier transform infrared spectroscopy (FT-IR) spectra of YVO_4:Eu and YVO_4:Eu/SiO_2 NCs. From the FT-IR spectra, it can be observed that the strong peak at 802 cm^{-1} and the weak peak at 453 cm^{-1} are apparently associated with the characteristic vibrational mode of V–O bond and Y–O bond, respectively [23]. The broad absorption band at 3411 cm^{-1} and a weak one at 1629 cm^{-1} can be assigned to the symmetrical stretching vibration and the bending vibration of H–O–H (H_2O molecules), respectively [24–25]. The peaks at 1392 and 1577 cm^{-1} are assigned to

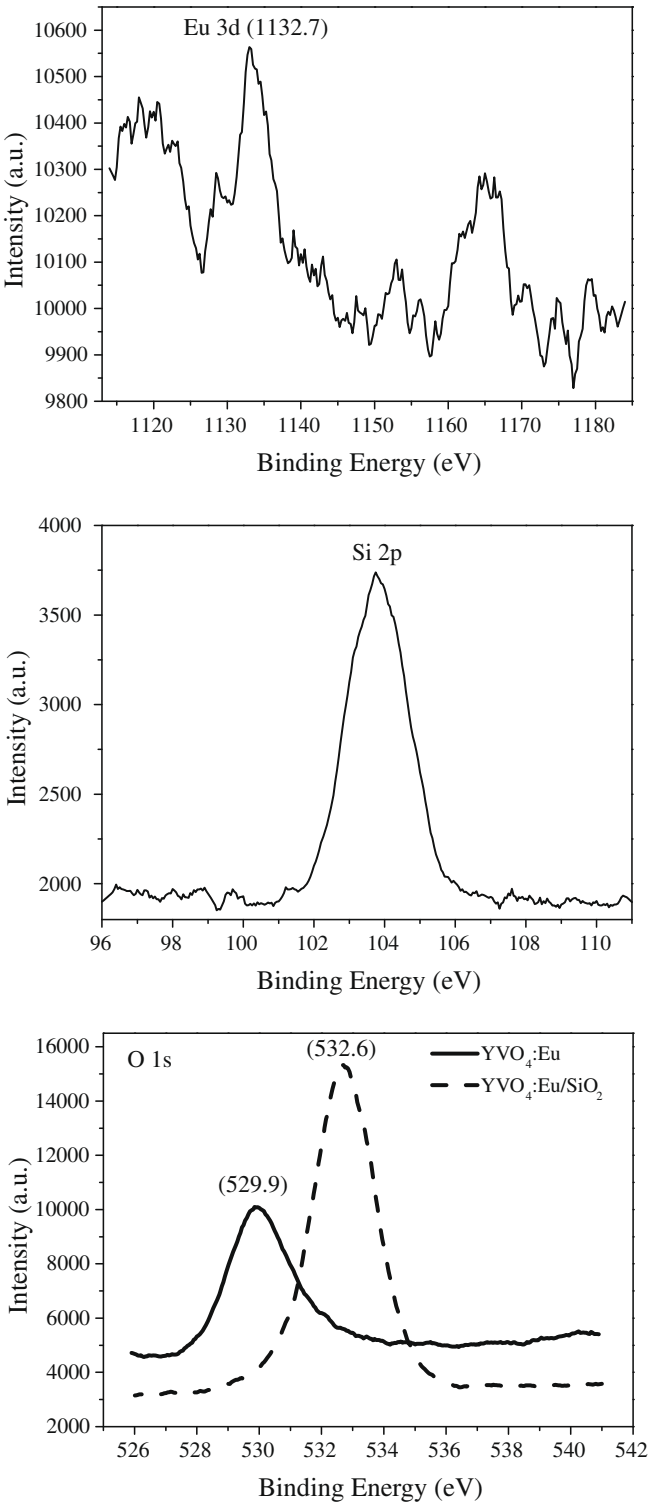

Fig. 3. XPS spectra of Eu 3d in YVO_4:Eu NCs, Si 2p in YVO_4:Eu/SiO_2 NCs and O 1s in YVO_4:Eu (solid line), YVO_4:Eu/SiO_2 NCs (dash line).

vibrations of the carboxylate anion in the citrate [24,26], which confirm the presence of the citrate ligands. The positions of these two bands were sensitive to the chemical compositions of the nanoparticle surfaces [27]. In addition, the two weak bands at 2924 and 2854 cm^{-1} correspond to the asymmetrical and symmetrical stretching vibrational modes of the CH_2 group, respectively [28–29]. In the case of silica-coated NCs (Fig. 4B), aside from the presence of the characteristic absorption bands, the strong

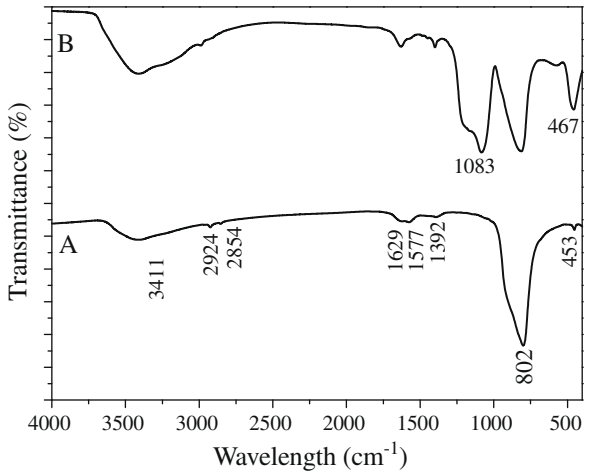

Fig. 4. FT-IR spectra of the YVO_4:Eu (A) and YVO_4:Eu/SiO_2 (B) NCs.

absorption peaks at 1083 and 467 cm^{-1} are attributed to Si–O–Si asymmetrical stretching vibration and Si–O bending vibration, respectively. The absorption band in the region of 3700–3000 cm^{-1} is stronger than that in the YVO_4:Eu NCs, which mainly bases on stretching vibration of –OH groups from silica shells. Due to the presence of the hydrophilic citrate ligands and silica shell, the YVO_4:Eu and YVO_4:Eu/SiO_2 NCs can be redispersed into water and keep stable for more than 24 h without any visible precipitate under ambient conditions.

The UV–vis absorption spectra of the samples are shown in Fig. 5. The broad band from 250 to 300 nm centered around 280 nm is attributed to a charge transfer from the oxygen ligands to the central vanadium atom inside of the VO_4^{3-} group. Under 280-nm UV excitation, colloidal YVO_4:Eu and YVO_4:Eu/SiO_2 NCs solutions exhibit strong red luminescence of Eu^{3+} ions (see Fig. 6, right). The excitation peaks corresponding to the europium emission of NCs (Fig. 6, left) agree well with the absorption peaks from the vanadate ions, while the Eu^{3+} ions have no absorption at the excitation wavelength of 280 nm. Therefore, it is clear that the emission from Eu^{3+} ions in the nanocrystals occurs after the energy transfer from the excited vanadate to the europium ions. The energy transfer process has been investigated by other authors [30–31].

The room-temperature emission spectra of YVO_4:Eu and YVO_4:Eu /SiO_2 NCs were measured in water with 0.125 mg/ml concentration. The most intense peak at 616 nm corresponds to

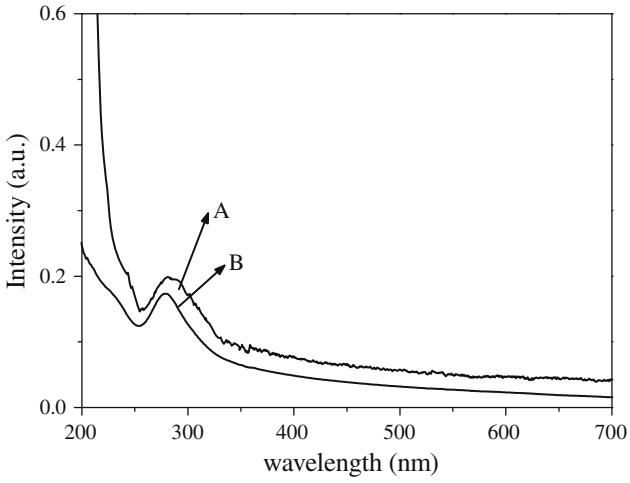

Fig. 5. UV–vis absorption spectra of the YVO_4:Eu NCs in ethanol (A) and YVO_4:Eu/SiO_2 NCs in water (B).

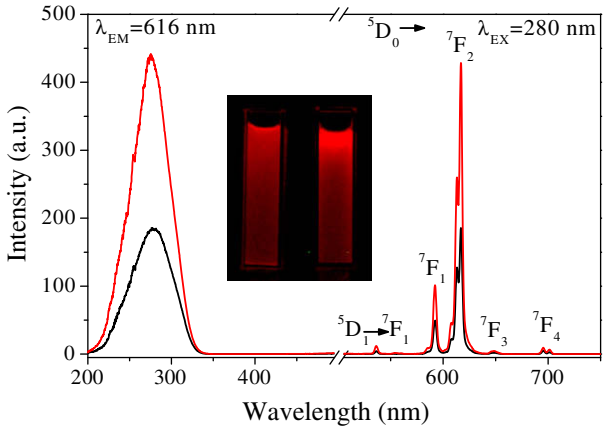

Fig. 6. Room-temperature excitation and emission spectra of YVO_4:Eu (bottom line) and YVO_4:Eu/SiO_2 (up line) aqueous solutions with 0.125 mg/ml NCs. Inset: Their luminescence photos photographed under 254-nm excitation.

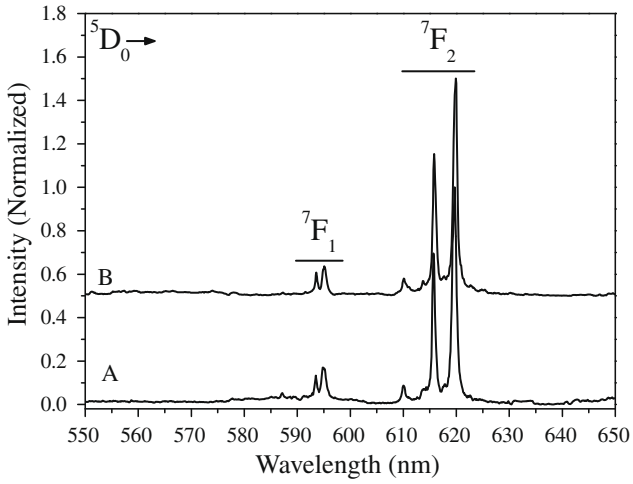

Fig. 7. Low-temperature emission spectra of YVO_4:Eu (A) and YVO_4:Eu/SiO_2 (B) NCs under 266-nm excitation.

$^5D_0 \rightarrow {}^7F_2$ forced electric-dipole transitions (Fig. 6, right). While the weak peaks at 535, 590, 650, and 700 nm correspond to the transitions of $^5D_1 \rightarrow {}^7F_1$, $^5D_0 \rightarrow {}^7F_1$, $^5D_0 \rightarrow {}^7F_3$, $^5D_0 \rightarrow {}^7F_4$, respectively. It is well-known that the $^5D_0 \rightarrow {}^7F_1$ transition is a typical magnetic dipole transition and usually taken as a standard transition because its intensity is independent to a large extent on the local environment. The electric-dipole transitions $^5D_0 \rightarrow {}^7F_2$ is a hypersensitive transition, which is allowed only on the condition that the europium ion occupy a site without an inversion center and very sensitive to the local environment [32–33]. In YVO_4:Eu NCs, the Eu^{3+} ions occupy the sites without inversion symmetry (D_{2d}), which results in the high luminescence intensity of $^5D_0 \rightarrow {}^7F_2$. The remarkable fluorescence enhancement of 2.17 times were observed for YVO_4:Eu/SiO_2 NCs. As we known, for rare-earth-doped materials, hydroxyls play a major role in fluorescence quenching [34–35]. When the NCs are dispersed in aqueous solutions, the surface of the NCs adsorbs a lot of hydroxyl species. After the YVO_4:Eu cores were coated by a shell of SiO_2, the emission intensity increased substantially. This is mainly because the SiO_2 on the surface of the NCs forms a protecting layer, which would effectively isolate the Eu^{3+} ions from water and thus reducing the deleterious effects of water on the luminescence yield.

In addition, surface defects also play important roles in quenching the luminescence of NCs due to the large surface-to-volume ratio of NCs. Based on experimental and theoretical studies, many reports have confirmed that surface and interior environments are different for RE ions doped in NCs [12–16,24,36–41]. In the following discussion, the Eu^{3+} ions were also used as a probe to investigate effect of the surface and coating on photoluminescence in YVO_4:Eu and YVO_4:Eu/SiO_2 NCs. The low-temperature (10 K) emission spectra of YVO_4:Eu and YVO_4:Eu/YVO_4/SiO_2 NCs excited with a 266-nm laser are presented in Fig. 7. The emission at 616 and 619 nm corresponds to Stark levels in the $^5D_0 \rightarrow {}^7F_2$ transition. Fig. 8 gives the low-temperature excitation spectra of $^5D_0 \rightarrow {}^7F_2$ fluorescence (619 nm), and there are two excitation peaks correspond to the $^7F_0 \rightarrow {}^5D_0$ transition. The $^5D_0$ and $^7F_0$ states do not split in the crystal field. Therefore, the emission and excitation transitions between $^5D_0$ and $^7F_0$ levels can be used to monitor the number of symmetry sites present in the lattice [9,13,14]. By frequency selective excitation, different Eu^{3+} luminescent centers can be distinguished if they exist. Note that the $^5D_0 \rightarrow {}^7F_0$ transition is strictly forbidden for Eu^{3+} ions occupying a site of D_{2d} symmetry in the single-crystalline YVO_4 [42], but becomes partially permitted in the YVO_4 powders [36]. In our experiments, the excitation band for $^7F_0 \rightarrow {}^5D_0$ transition presents two peaks clearly

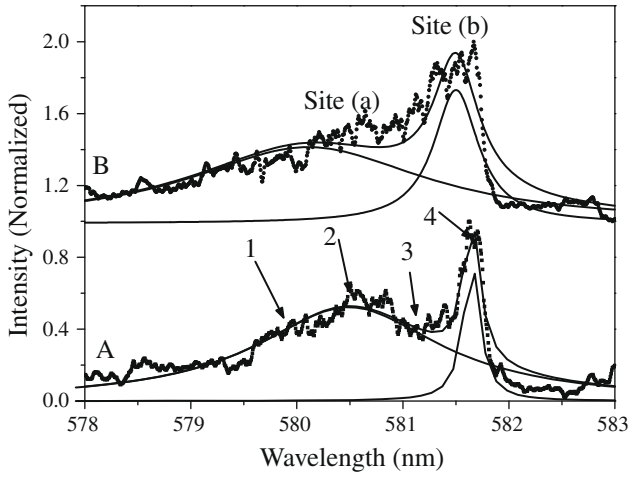

Fig. 8. Low-temperature excitation spectra of $^7F_0 \rightarrow {}^5D_0$ (monitored at 619 nm) for YVO_4:Eu (A) and YVO_4:Eu/SiO_2 (B) NCs. Each of them can be deconvolved into two Gaussian peaks.

(marked as site (a) and site (b)). The peak of site (a) has a long tail extending to the high-energy side, and also its linewidth is broader than that of site (b). The site-selective emission spectra were recorded by using different resonant excitation wavelengths in the $^7F_0 \rightarrow {}^5D_0$ absorption bands (labeled as 1–4 in Fig. 8), as shown in Fig. 9. The difference in spectral configuration among the emission spectra is apparent. Spectra 1, 2, and 3 were obtained by exciting different positions of site (a). The Stark splitting cannot be discerned clearly from the spectra. We propose that site (a) is an emission center on the NCs surface. The Eu^{3+} ions on the surface locate at various symmetrical sites because the surface states modify the site symmetry irregularly. Spectra 4 were taken by exciting at site (b), exhibiting two clear peaks centered at 616 and 619 nm and indicating that site (b) originates from an emission center in a crystalline environment. According to the low-temperature emission spectra, these two peaks are attributed to the Stark splitting of $^5D_0 \rightarrow {}^7F_2$ transition, so we conclude that the site (b) is an interior center in the NCs. The $^7F_0 \rightarrow {}^5D_0$ absorption bands of samples (Fig. 7) are deconvolved into two individual Gaussian peaks. From which one can see that the intensity ratios of these two peaks are different in these samples. The intensity ratios of site (a) to site (b) are 5.82 and 2.33 for YVO_4:Eu and YVO_4:Eu /SiO_2 NCs, respectively.

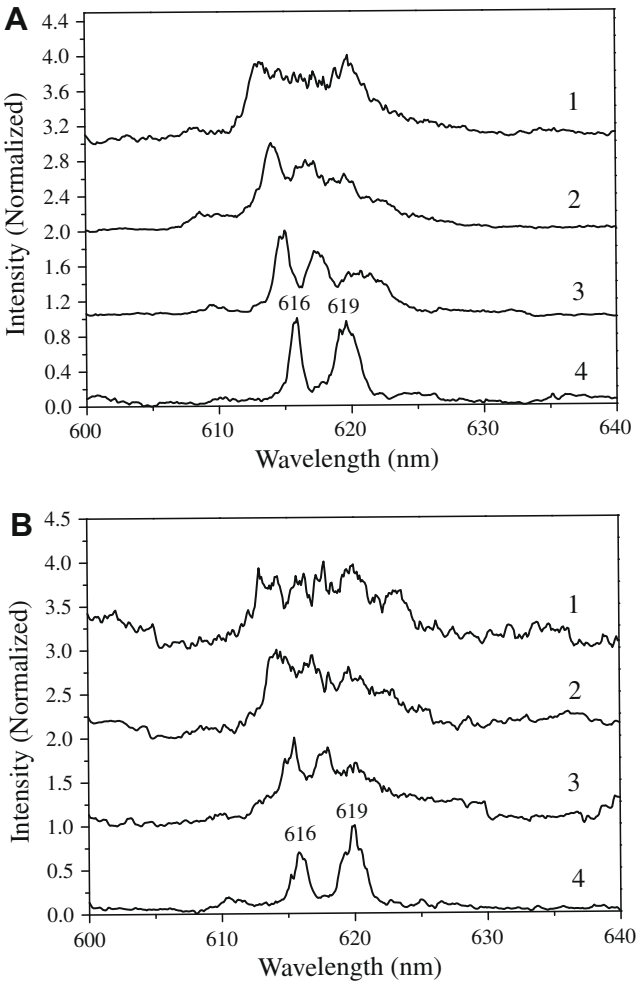

Fig. 9. Emission spectra of nanospheres corresponding to different excitation positions in Fig. 8. (A) YVO_4:Eu NCs and (B) YVO_4:Eu/SiO_2 NCs.

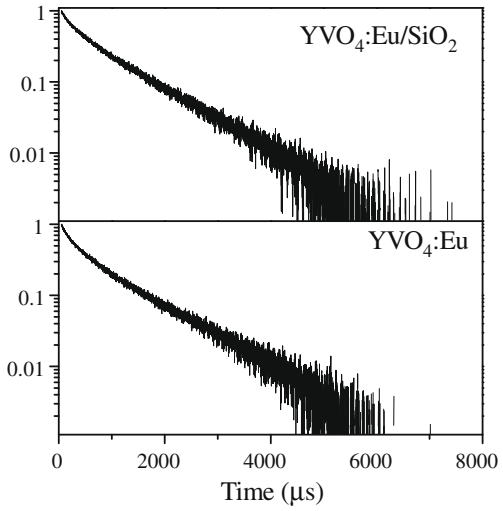

Fig. 10. Room-temperature luminescence decay curves of YVO_4:Eu and YVO_4:Eu/SiO_2 NCs under 266-nm excitation.

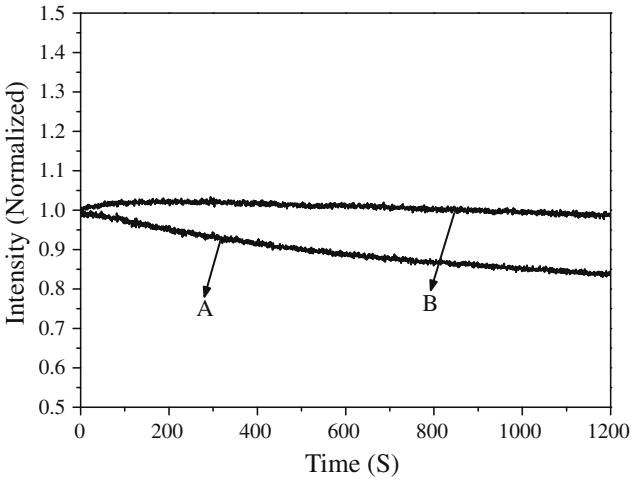

Fig. 11. Photobleaching effect of YVO_4:Eu (A) and YVO_4:Eu/SiO_2 (B) NCs under continuous 280-nm irradiation.

This indicates that the SiO_2 shells effectively reduce the surface defects of YVO_4:Eu NCs and the modification of surface results in the enhancement of luminescence intensity.

Luminescence lifetime is a key parameter for luminescence probe. Considering that all possible applications of luminescent probes for bio-detection should be carried out at room temperature, the room-temperature luminescence decay curves of $^5D_0$ energy level in two samples under 266-nm excitation are measured and shown in Fig. 10. The average luminescent lifetimes of YVO_4:Eu and YVO_4:Eu/SiO_2 NCs are 749 μs and 884 μs, respectively. The increased lifetime is observed in YVO_4:Eu/SiO_2 NCs, as compared to that of YVO_4:Eu NCs. Knowing that the measured lifetime (τ) is related to the radiative (τ_r) and nonradiative lifetime (τ_{nr}). Obviously, the surface modification decreases the nonradiative processes and increases the luminescent lifetime of Eu^{3+} ions. Photostability is another key parameter for luminescent probes. The photobleaching experiments of YVO_4:Eu and YVO_4:Eu/SiO_2 NCs were carried out in water (Fig. 11). It was observed that the fluorescence intensity from the YVO_4:Eu NCs solution decreased by approximately 16.1% in 20 min, whereas the fluorescence intensities of the YVO_4:Eu/SiO_2 NCs solutions showed only 3.9% decrease in the same time. Interestingly, a little increase was observed in the sample YVO_4:Eu/SiO_2 in the first 3 min. The reason for this phenomenon is current under investigation. The high photostability of the enveloped nanoparticles should be arisen from the isolation of the Eu^{3+} from the outside environment by a layer of hydrolyzed SiO_2, which shield the Eu^{3+} from solvent molecules and free radicals caused by light exposure and effectively protect the molecules from photodecomposition.

4. Conclusion

In summary, the water-soluble YVO_4:Eu and YVO_4:Eu/SiO_2 colloidal NCs were synthesized successfully. FT-IR spectra confirmed that the citrate ligands presented on the surface of the NCs, which make these NCs dispersable in water and cause the formation of transparent solutions. After the YVO_4:Eu NCs were coated with SiO_2, a protecting layer formed on the NCs surface and reduced the fluorescence quenching from water molecules. The laser selective excitation spectra confirm that there are two kinds of luminescent centers, inner Eu^{3+} ions and surface Eu^{3+} ions in the both two samples. The SiO_2 shell modified the surface of YVO_4:Eu NCs and enhanced the luminescence intensity. The dynamic analysis at room temperature and photobleaching experiments indicate that the YVO_4:Eu/SiO_2 NCs have longer lifetime and higher photostability. These features are very attractive for exploitation of fluorescent bio-probes. By incorporating different RE ions into the YVO_4 lattice

different color emission will be obtained, for example, up-conversion fluorescence NCs doped with Er^{3+} ions [4,43], which means that these core/shell NCs may find their practical applications in biology.

Acknowledgements

This work was supported by the National Natural Science Foundation of China (Grant Nos. 10474096 and 50672030).

References

[1] A.K. Levine, F.C. Palilla, Appl. Phys. Lett. 5 (1964) 118.
[2] A. Huignard, V. Buissette, G. Laurent, T. Gacoin, J.P. Boilot, Chem. Mater. 14 (2002) 2264.
[3] K. Riwotzki, M.J. Haase, Phys. Chem. B 102 (1998) 10129.
[4] Y. Sun, H. Liu, X. Wang, X. Kong, H. Zhang, Chem. Mater. 18 (2006) 2726.
[5] H. Xu, H. Wang, Y. Meng, H. Yan, Solid State Commun. 130 (2004) 465.
[6] L. Sun, Y. Zhang, J. Zhang, C. Yan, C. Liao, Y. Lu, Solid State Commun. 124 (2002) 35.
[7] W. DeW. Harrocks Jr., G.R. Schmidt, D.R. Sudnick, C. Kittrel, R.A. Bernheim, J. Am. Chem. Soc. 99 (1977) 2378.
[8] W. DeW. Harrocks Jr., D.R. Sudnick, Science 206 (1979) 1194.
[9] W. DeW. Harrocks Jr., D.R. Sudnick, Acc. Chem. Res. 14 (1981) 384.
[10] R.C. Hole, W. DeW. Harrocks Jr., Inorg. Chim. Acta 171 (1990) 193.
[11] S.T. Frey, C.A. Chang, K.L. Pounds, W. DeW. Harrocks Jr., Inorg. Chem. 33 (1994) 2882.
[12] Z. Wei, X. Mei, Z. Wei, Y. Min, Q. Ming, X. Sahang, C. Garapon, Chem. Phys. Lett. 376 (2003) 318.
[13] C. Wu, W. Qin, G. Qin, D. Zhao, J. Zhang, S. Huang, Appl. Phys. Lett. 82 (2003) 520.
[14] X. Jiang, C. Yan, L. Sun, Z. Wei, C. Liao, J. Solid State Chem. 175 (2003) 245.
[15] K. Riwotzki, H. Meyssamy, A. Kornowski, M. Haase, J. Phys. Chem. B 104 (2000) 2824.
[16] K. Riwotzki, H. Meyssamy, A. Schnablegger, A. Kornowski, M. Haase, Angew. Chem. Int. Ed. 40 (2001) 573.
[17] L.M. Liz-Marzán, P. Mulvaney, J. Phys. Chem. B 107 (2003) 7312.
[18] M. Darbandi, W. Hoheise, T. Nann, Nanotechnology 7 (2006) 4168.
[19] W. Stöber, A. Fink, E. Bohn, J. Colloid Interf. Sci. 26 (1968) 62.
[20] N.S. Ramgir, I.S. Mulla, K.P. Vijayamohanan, J. Phys. Chem. B 109 (2005) 12297.
[21] W.S. Epling, C.K. Mount, G.B. Hoflund, Appl. Surf. Sci. 134 (1998) 187.
[22] T. Moon, S. Hwang, D. Jung, D. Son, C. Kim, J. Kim, M. Kang, B. Park, J. Phys. Chem. C 111 (2007) 4164.
[23] S. Hirano, T. Yogo, K. Kikuta, W. Sakamoto, H. Koganei, J. Am. Chem. Soc. 79 (1996) 3041.
[24] D. Lin-Vien et al., The Handbook of IR and Raman Characteristic Frequencies of Organic Molecules, Academic Press, New York, 1991.
[25] H. Hiramatsu, F.E. Osterloh, Langmuir 19 (2003) 7003.
[26] Y. Wang, X. Teng, J. Wang, H. Yang, Nano Lett. 3 (2003) 790.
[27] W. Wang, X. Chen, S. Efrima, J. Phys. Chem. B 103 (1999) 7238.
[28] N.B. Clothup, L.H. Daly, S.E. Wiberley, Introduction to Infrared and Raman Spectroscopy, second ed., Academic Press, New York, 1975.
[29] G. Socrates, Infrared Characteristic Group Frequencies;, Wiley, New York, 1980.
[30] A. Huignard, V. Buissette, A. Franville, T. Gacoin, J. Boilot, J. Phys. Chem. B 107 (2003) 6754.
[31] K. Riwotzki, M. Haase, J. Phys. Chem. B 105 (2001) 12709.
[32] B.R. Judd, Phys. Rev. 127 (1962) 750.
[33] G.S. Ofelt, J. Chem. Phys. 37 (1962) 511.
[34] W. Di, X. Wang, B. Chen, S. Lü, X. Zhao, J. Phys. Chem. B 109 (2005) 13154.
[35] S. Banerjee, L. Huebner, M.D. Romanelli, G.A. Kumar, R.E. Riman, T.J. Emge, J.G. Brennan, J. Am. Chem. Soc. 127 (2005) 15900.
[36] C. Yan, L. Sun, C. Liao, Y. Zhang, Y. Lu, S. Huang, S. Lü, Appl. Phys. Lett. 82 (2003) 3511.
[37] V. Sudarsan, F.C.J.M. van Veggel, R.A. Herring, M. Raudsepp, J. Mater. Chem 15 (2005) 1332.
[38] J.W. Stouwdam, F.C.J.M. van Veggel, Langmuir 20 (2004) 11763.
[39] G.A. Hebbink, J.W. Stouwdam, D.N. Reinhoudt, F.C.J.M. van Veggel, Adv. Mater. 14 (2002) 1147.
[40] J.W. Stouwdam, F.C.J.M. van Veggel, Nano Lett. 2 (2002) 733.
[41] J.W. Stouwdam, G.A. Hebbink, J. Huskens, F.C.J.M. van Veggel, Chem. Mater. 15 (2003) 4604.
[42] C. Brecher, H. Samelson, A. Lempicki, R. Riley, T. Peters, Phys. Rev. 155 (1967) 178.
[43] F. Wang, X. Xue, X. Liu, Angew. Chem. Int. Ed. 47 (2008) 906.